Hindawi
Geofluids
Volume 2022, Article ID 6231192, 14 pages
https://doi.org/10.1155/2022/6231192

Research Article

Pore Structure of Oil Shale Heated by Using Conduction and Microwave Radiation: A Case Study of Oil Shale from the Fushun in China

Yao Cheng,[1] **Shan Lin**,[2] **and Yulin Ma**[2]

[1]*College of Innovation and Practice, Liaoning Technical University, Fuxin 123000, China*
[2]*School of Mechanics and Engineering, Liaoning Technical University, Fuxin 123000, China*

Correspondence should be addressed to Yao Cheng; yaoyao9873@163.com

Received 8 January 2022; Accepted 15 April 2022; Published 2 June 2022

Academic Editor: Yu Zhao

To examine the evolution of the internal pore structure of and the law of changes in oil shale under different heating modes but at the same temperature, this study subjected φ20 mm × 20 mm specimens of oil shale to temperatures in the range of 20°C ~500°C by using a muffle furnace and a microwave pyrolysis device. We carried out experiments on the pyrolysis reaction under different temperatures and used scanning electron microscopy, backscattering, the mercury intrusion test, and MATLAB for a refined characterization of the specimens. The results showed that the microwave pyrolysis of oil shale was much shorter than its conduction-induced heating. As the microwave power increased, the time required to reach the target temperature decreased. The phenomenon of "hole blocking" was observed at 400°C ~500°C during conduction-based heating but did not occur in the microwave pyrolysis of oil shale. The porosity of oil shale heated by conduction was 3.4 times higher than its original porosity, whereas that of oil shale heated by microwave radiation was 4.9 times higher than its original value. It can be seen that compared with conduction heating, radiant heating makes the pyrolysis of organic matter in oil shale more complete. During the pyrolysis process of oil shale, the complete reaction of organic matter causes the thermal fracture of the oil shale to produce a large number of pores and interconnected cracks. Thereby, a seepage channel for pyrolysis gas and oil is formed, and the recovery rate of oil and gas is increased.

1. Introduction

Oil shale is an unconventional source of oil and gas that, like natural gas and coal, is a nonrenewable source of energy. It is a sedimentary rock with high ash content and combustible organic matter. Global oil shale reserves can be converted into one trillion tons of shale oil, about 4.3 times higher than the recoverable oil reserves of 230.58 billion tons [1–5]. China accounts for about 7% of the world's oil shale reserves, distributed mainly in the northeast and northwest regions of the country.

The microwave retorting of oil shale is an effective method to produce shale oil. Compared with the conventional dry distillation method, it has the advantages of fast and uniform heating as well as the absence of a temperature gradient. The oil and gas produced by the pyrolysis of oil shale are mainly derived from organic matter [6]. After pyrolysis, pores or cracks are formed in the original location of the organic matter that are conducive to the transmission of microwaves in the layer of oil shale through the expansion of the area that is heated. The cracks formed are also beneficial for the drainage and production of shale oil. The minerals in oil shale also produce a series of physical and chemical reactions under high temperature that affect the characteristics of the pore structure of its solid skeleton. The structural characteristics of the solid skeleton of oil shale determine the rate of production of oil and gas products. In particular, in the in situ thermal injection-based production

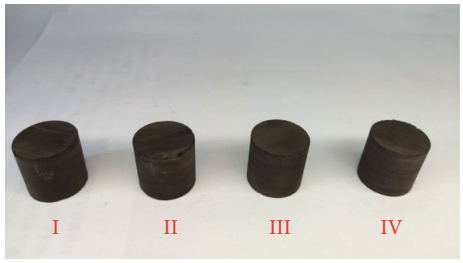

Figure 1: Oil shale specimens.

of oil shale, the pore structure of the solid skeleton after pyrolysis and the interconnectivity of the pores are the main factors affecting production [7].

The pyrolysis of oil shale involves a series of complex endothermic chemical reactions. The distribution and evolution of its internal structure during pyrolysis play a vital role in the formation and escape of the products. Many researchers have studied the pore and fracture structures of oil shale before and after pyrolysis through various methods. Saif et al. [8] analyzed changes in the porosity and connectivity of oil shale during pyrolysis. They observed that connected pores had developed at a microscopic scale along the kerogen-enriched layered structure. Tiwari et al. [9] used microcomputed tomography (CT) technology to study the pore structure of oil shale before and after pyrolysis and observed that a new and larger fracture channel was created after pyrolysis. The size of the pores was related to the distribution of kerogen. Kang et al. [10] studied changes in the porosity of oil shale during its pyrolysis. They used Fushun oil shale in China as an example and obtained the rate equation of its pyrolysis by using its thermal curve to establish a quantitative model of its porosity by assuming that changes in it were caused by the high-temperature pyrolysis of kerogen. Liu et al. [11] used thermogravimetric analysis and cryogenic nitrogen adsorption to quantitatively analyze its pore structure under different pressures and final pyrolysis temperatures. The evolution of the pore structure of oil shale involves complex physical and chemical processes. It is the result of the interaction of organic matter, pyrolysis products, and inorganic minerals. The pyrolysis of organic matter increases the specific surface area and pore volume of oil shale. Meng et al. [12] used micro-CT to analyze the process of crack development in oil shale during pyrolysis based on thermoelastic mechanics theory and experiments. They found that the main cause of fracture was thermal stress when the temperature of oil shale was less than 300°C. When its temperature exceeded 300°C, the fracture mechanism of oil shale was dominated by the expansion pressure caused by the pyrolysis of organic matter. Bai et al. [13] used a variety of experimental methods to study the thermal effects and physical and chemical properties of oil shale. A pyrolysis experiment on Huadian oil shale at 100°C~800°C showed that temperature had a significant influence on the production of the products of pyrolysis and changes in pore structure. The main stage of the decomposition of kerogen occurred at 350°C~500°C. The smaller the size of the pores was, the more complex was their structure. Harfi et al. [14] concluded from experiments on the pyrolysis of Tarfaya oil shale in Morocco that compared with conventional methods of pyrolysis, the oil obtained after microwave heating was less polar and contained less sulfur and nitrogen. By studying the influence of microwave power on oil shale pyrolysis, it is concluded that with the increase of microwave power, the time required to reach the maximum temperature is gradually shortened, the final pyrolysis temperature can reach 800°C, and the semicoke yield decreases with the increase of microwave power [15]. At the same time, the shale oil production rate first increases and then decreases, the maximum value is 13.5%, and the dry distillate gas production rate continues to increase. Lee et al. [16] compared the effects of the microwave dry distillation and conventional dry distillation of oil shale and found that the shale oil obtained by microwave dry distillation had higher hydrocarbon content (better quality), low sulfur and nitrogen content, a higher light component, and a better hydrogenation effect. Wang et al. [17] studied the characteristics of heating of oil shale and semicoke using microwaves and discussed the characteristics of the pyrolysis of the mixture from the perspectives of their mixing ratio, the microwave power, and particle size. The above review showed that comparative studies on changes in the internal pore and fissure structures of oil shale through conduction and radiation were lacking. However, the influence of different heating modes of conduction and radiation on the change of oil shale pore structure will directly determine the choice of in situ pyrolysis method.

This study used the Fushun East Open-Pit Mine as a research object. We used experiments on high-temperature pyrolysis and microwave pyrolysis, scanning electron microscopy (SEM), backscattering, and the mercury injection test to analyze the characteristics of evolution of the pore structure of shale and laws of changes in it under different modes of heating. By comparing two different ways of pyrolyzing oil shale, the principle of different ways of pyrolyzing oil shale is analyzed. The authors obtained the best way to pyrolyze oil shale and then analyzed the pores and fractures generated by organic matter in oil shale in the process of different pyrolysis methods. The authors also analyzed the pyrolysis of organic matter in the cracks of oil shale.

2. Experimental Equipment and Methods

2.1. Experimental Samples. The materials and methods section should contain sufficient detail so that all procedures can be repeated. It may be divided into headed subsections if several methods are described. The oil shale samples for this test were taken from the Fushun East Open-Pit Mine. They were sealed with paraffin on site and transported back to the laboratory. We used a wire saw to drill four cylindrical specimens of size φ20 mm × 20 mm along the vertical direction of bedding of the oil shale; they are presented in Figure 1. The average mass of the specimens was 15.26 g, and their average density was 2.43 g/cm^3. The axial direction of the test piece was perpendicular to the bedding, and both its ends were smoothed with sandpaper. The Fushun oil

Table 1: Fushun oil shale industry analysis and aluminum retort analysis.

Analysis parameters	Industrial analysis				Fisher analysis			
	Moisture	Ash	Volatile	Fixed carbon	Oil production	Water yield	Residue	Stress loss
Content%	2.88	77.19	17.76	2.17	6.02	4.44	85.60	3.94

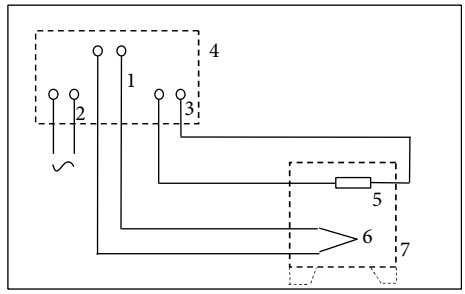

Figure 2: Muffle furnace equipment. (1) Thermocouple. (2) Power supply. (3) Electric furnace. (4) Controller. (5) Electric heating element. (6) Thermocouple. (7) High-temperature electric furnace.

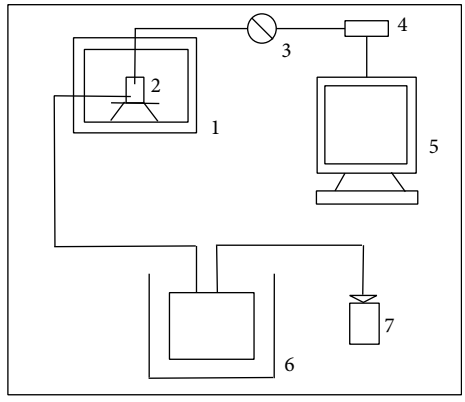

Figure 3: Schematic diagram of microwave pyrolysis. (1) Microwave generator. (2) Quartz glass. (3) Thermocouple. (4) Data acquisition instrument. (5) Computer. (6) Condenser. (7) Gas cylinder.

shale industry analysis and aluminum retort analysis in Table 1.

2.2. Experimental Equipment. The high-temperature pyrolysis experiment involved a high-precision temperature-controlled SX2-12-12A muffle furnace. An electric heating rod was used to heat the kettle and had a maximum temperature of 1200°C, a heating rate of 15°C/min, a working voltage of 380 V, and a rated power was 12 kW. The microwave reactor used in the experiment was a restructured G80F23CSL-A9 (SO) microwave oven. The microwave output power was 800 W, and the frequency was 2450 MHz. The principle of muffle furnace equipment is presented in Figure 2.

The experimental device for microwave pyrolysis consisted of an experimental pyrolysis device, a product cooling device, and a product collection device. The experimental pyrolysis device was composed of three parts: a pyrolysis reactor made of quartz glass, a microwave oven, and a temperature control system. The microwave generator used was a reformed Midea microwave oven with an output power of 400 W and frequency of 2450 MHz. The cooling system was composed of a condenser tube as product cooling device, cold trap, and low-temperature cooling circulation pump to cool the products of pyrolysis. The product collection device was composed of a gas pipe, a conical flask, and an airbag to collect liquid and gaseous products. The schematic diagram of microwave pyrolysis is presented in Figure 3.

In the experiment, a scanning electron microscope (QUANTA250) was used to scan. The principle of SEM was to use a very thin electron beam to scan the specimen to display a stereoscopic image of its surface structure synchronized with the electron beam. The magnification of the SEM image was defined as the ratio of its width to the scanning width of the electron beam in the corresponding direction on the sample. The magnifications used in this experiment were 500x, 1000x, 2000x, and 4000x. During the experiment, the sample was fixed on a platform using conductive tape and was observed and analyzed after blowing and spraying gold on it.

2.3. Experimental Procedure. We first performed SEM and backscatter scanning at room temperature and then moved specimens No. I and II into the muffle furnace. According to the literature [18, 19], 300°C is the temperature at which the organic matter of Fushan oil shale begins to undergo pyrolysis, and at which temperature, its porosity suddenly increases. Therefore, the initial temperature was set to 300°C for 30 min. After they had naturally cooled to room temperature, we subjected the specimens to SEM and the mercury intrusion test. The experimental temperature was increased at intervals of 100°C to 500°C, and the above experimental steps were repeated. Specimens No. III and IV were then placed into the 100 mL quartz glass reactor. Its power was adjusted to reach the target temperature of 300°C. This temperature was maintained for 30 min, following which the microwave pyrolysis device was turned off. After they had naturally cooled to room temperature, the test pieces were taken out and subjected to SEM and the mercury intrusion test. The experimental temperature was increased at intervals of 100°C to 500°C, and the above experimental steps were repeated. During the pyrolysis experiment, nitrogen was used as a protective gas to avoid the oxidation of oil shale and improve the accuracy of the results.

3. Experimental Results and Analysis

3.1. SEM/BSE Morphology. Scanning electron microscopy can show details of the mesostructure of the substance and

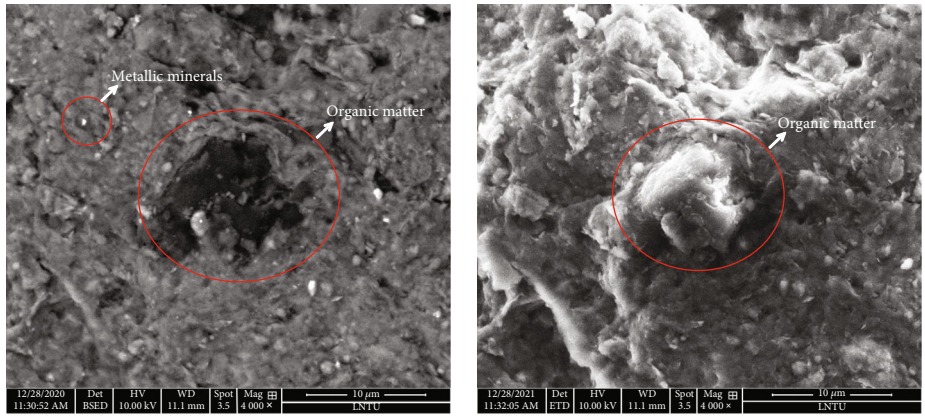

(a) (b)

Figure 4: (a) Backscatter image at the same position. (b) SEM image at the same position.

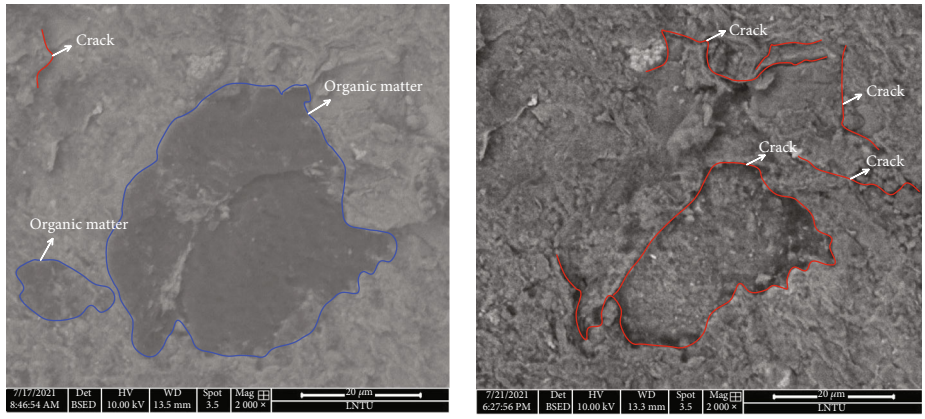

(a) (b)

Figure 5: Backscattering image of oil shale at (a) 20°C and (b) 500°C at the same location.

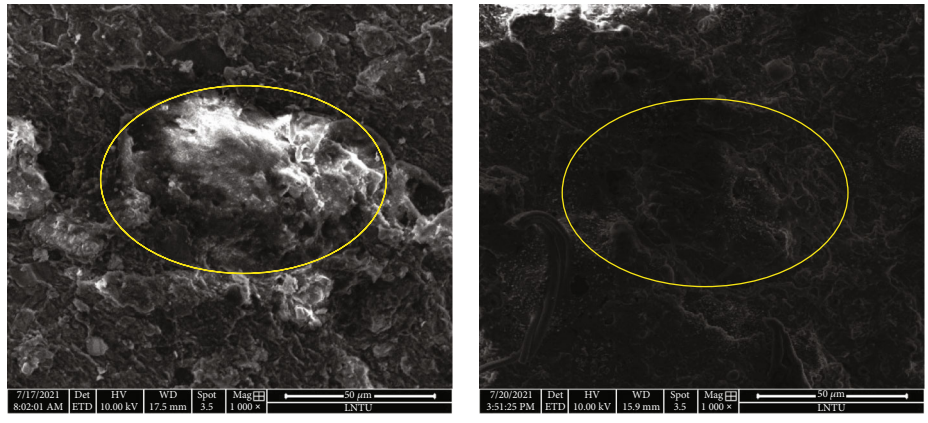

(a) (b)

Figure 6: SEM image of oil shale at (a) 20°C and (b) 500°C at the same location.

is important for analyzing the internal morphology and composition of mineral particles. The range of magnification of the SEM can be extended from the scale of observation of the optical microscope to the nanometer scale, and this can be used to directly observe various uneven microstructures on the surface of the test piece. The principle of backscattered electron imaging (BSE) is to use the atomic number to correspond to images with different brightness values.

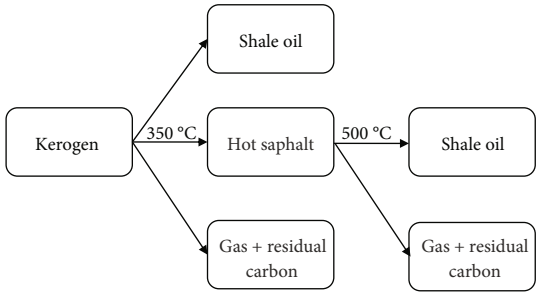

Figure 7: Flowchart of the pyrolysis of oil shale.

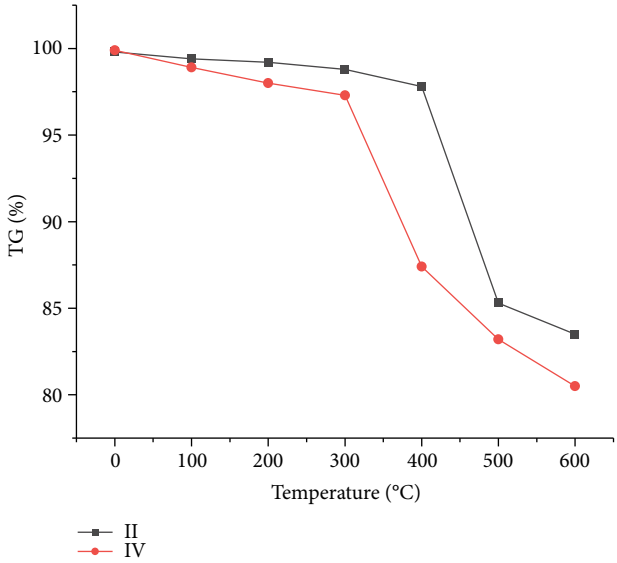

Figure 8: TG map of oil shale specimens No. II and IV.

The higher the number is, the greater the brightness is. Usually, metallic minerals are the brightest and organic matter is the dimmest. Using this rule, BSE can be used to easily distinguish between organic matter and inorganic minerals [20].

Figure 4 shows that the organic matter was placed flat on its natural cross-section, had no fixed shape, interacted with the minerals, and had a nanospherical structure. The surface of Fushun oil shale was covered by many scattered flaky kaolinites and had a prominent bedding structure. In the original state, the internal structure of the oil shale was relatively dense and the pores were not significantly developed. However, Figures 5 and 6 show that as the temperature rose, pores inside the oil shale increased in number and became easier to identify. This was only a qualitative description and could not accurately reflect changes in the pores [21–25]. The backscattered electron image was the dimmest: black, alternating with minerals, and without a fixed shape. At the micron level, the organic matter was striped and bulky, its edges were irregular, and its shape was limited by the minerals, that is, there were no morphological components. Many internal nanopores were observed that were mainly interactive.

3.2. Distribution of Organic Matter. The organic matter in oil shale consists of mostly kerogen (parent material) and a small amount of bitumen. Although the pyrolysis of oil shale is affected by many factors, such as type and operating parameters of oil shale, it can be divided into two basic steps. As is shown in Figure 7, kerogen first depolymerized to form an intermediate-phase hot asphalt, a small amount of shale oil, pyrolysis gas, and residual carbon. The hot asphalt was the benzene-extracted organic matter remaining in the shale. As the temperature rose, the hot asphalt in the mesophase was further decomposed to produce shale oil, heat, and residual carbon. Although kerogen was found in different geological structures, the temperatures at which different kerogens were active and destroyed were similar, and ranged from 340°C to 360°C [26–30].

The curve of the loss of weight of the oil shale samples during pyrolysis with changes in temperature (TG map) was drawn according to their weights before and after heating using different pyrolysis methods. Figure 8 shows that the loss of weight of the samples under conduction-based heating and radiation-based heating was divided into two stages: low-temperature weight loss (20°C~300°C) and high-temperature weight loss (300°C~600°C). The low-temperature weight loss stage featured free water and partially bound water in oil shale, with a weight loss ratio less than 1% in the stage of softening of organic matter in oil shale in this temperature range. The high-temperature weight loss stage consisted of the pyrolysis of organic matter inside the oil shale, with a weight loss ratio of 19.74%. The reaction was most severe at 400°C~500°C, when the weight loss ratio was 14.43%. The SEM experiment and mercury injection experiment were conducted at temperatures of 20°C, 300°C, 400°C, and 500°C. The quality of specimens No. II and IV decreased significantly after being heated by conduction and microwaves. As shown in Figure 4, the mass of specimen No. II before heating was 50 g and decreased to 41.75 g after conduction-based heating. The rate of weight loss was 16.5%. The original mass of specimen No. IV was 50 g and decreased to 40.13 g after microwave heating, a rate of weight loss of 19.74%. It is clear from the figure that the efficiency of pyrolysis of microwave heating was significantly higher than that of conduction. The difference in weight loss between them was about 3.24%, indicating that some organic matter in the oil shale had not been fully pyrolyzed after conduction.

The image size and image color obtained by SEM observation are expressed by pixels and grayscale, respectively, and the grayscale is quantitatively controlled by a threshold value, which ranges from 0 to 255. When the threshold value is 0, it represents the deepest color of the image, and when the threshold value is 255, it represents the lightest color of the image, and the middle is the transition section. By colorizing the grayscale image, the content contained in the grayscale image can be more effectively displayed by using rich color contrast information, so that it can be better compared and analyzed with the original image. The blue area in the colorized grayscale distribution image represents the distribution of organic matter in oil shale, and the red area represents the distribution of oil shale pores and fractures. A

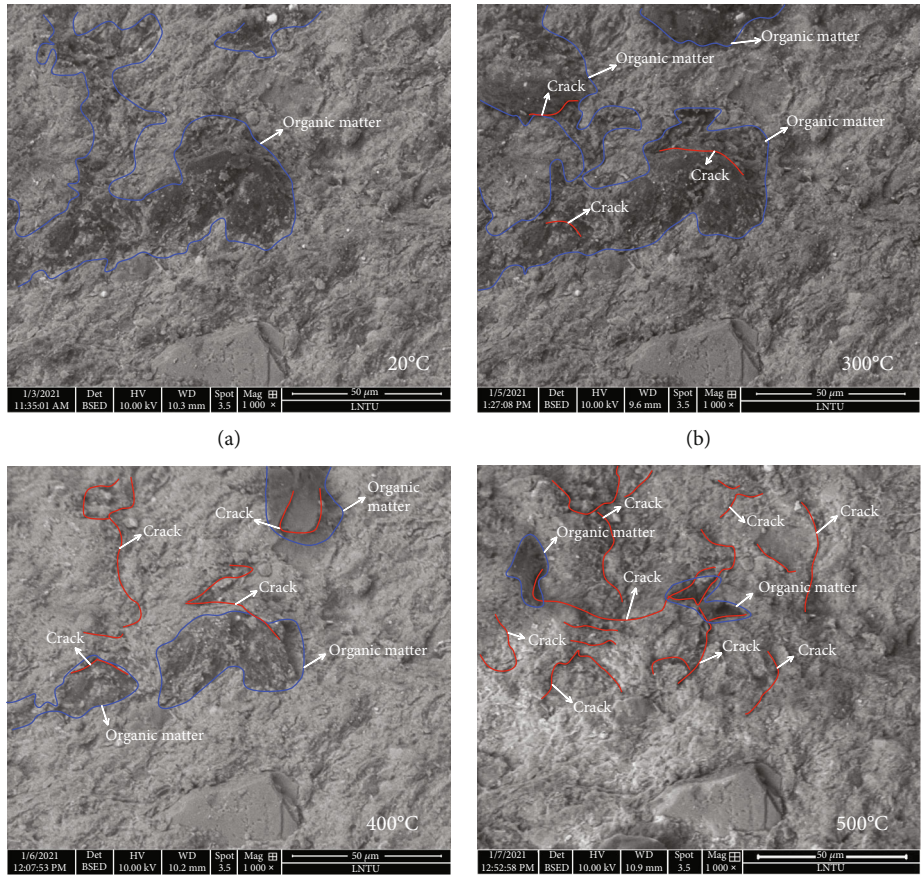

Figure 9: SEM images of oil shale before and after conduction-based heating. (a) Oil shale in the initial state. (b) Oil shale at 300°C. (c) Oil shale at 400°C. (d) Oil shale at 500°C.

binary space grayscale pore calculation model is established. Using the idea of two-dimensional integration, we first obtain the area of irregular pores. The corresponding height is obtained by using the threshold difference between the upper and lower sections with the farthest irregular pore distance. The pore volume is obtained by multiplying the corresponding height by the pore area.

Below are the images of the conduction heating and microwave heating effects observed by SEM and processed by MATLAB. Grayscale images have multilevel color depths between black and white. Through the colorization of grayscale images, the content contained in the grayscale images can be displayed more effectively, with rich color contrast information, which can better match it. The original image is compared and analyzed. In the color/gray distribution of the image, the blue area represents the distribution of organic matter in oil shale and the red area represents that of pore fractures. A visual analysis of the gray distribution map shows the development, connection, and distribution of pore fractures in oil shale as well as the degree of damage to it before and after heating.

The experimental process is shown in Figures 9 and 10. The oil shale specimens heated through conduction developed large cracks, and organic matter inside the oil shale ruptured because it decomposed into make gaseous or liquid material, which increased its porosity and provided a path for seepage. Thermal fracture during heating increased the porosity of oil shale. The above pyrolysis and rupture processes formed new pores and cracks in oil shale that interconnected to form channels conducive to flow and increased permeability. Figure 9 shows the pore distribution.

Figures 11 and 12 show that the organic matter flowed as a mixture of oil and gas as the temperature rose. When the temperature reached 300°C during microwave heating, the organic matter turned into hot bitumen and adhered to the pores and cracks of the oil shale. Microwave heating has the characteristic of selective heating. The area without organic matter heated up more quickly than areas containing organic matter. The duration of retention of bitumen was very short; some of it was even directly converted into shale oil and migrated along the cracks. At 400°C, the amount of organic matter decreased. According to the static display at different temperatures shown in Figure 11, the pores and cracks were generated during the flow of oil and gas, and the production of which was complete at 500°C. The effect of microwave heating was more prominent than that of conductive heating.

3.3. Law of Distribution of Pore Structure. According to the Hodot classification [31], the pore structures were divided

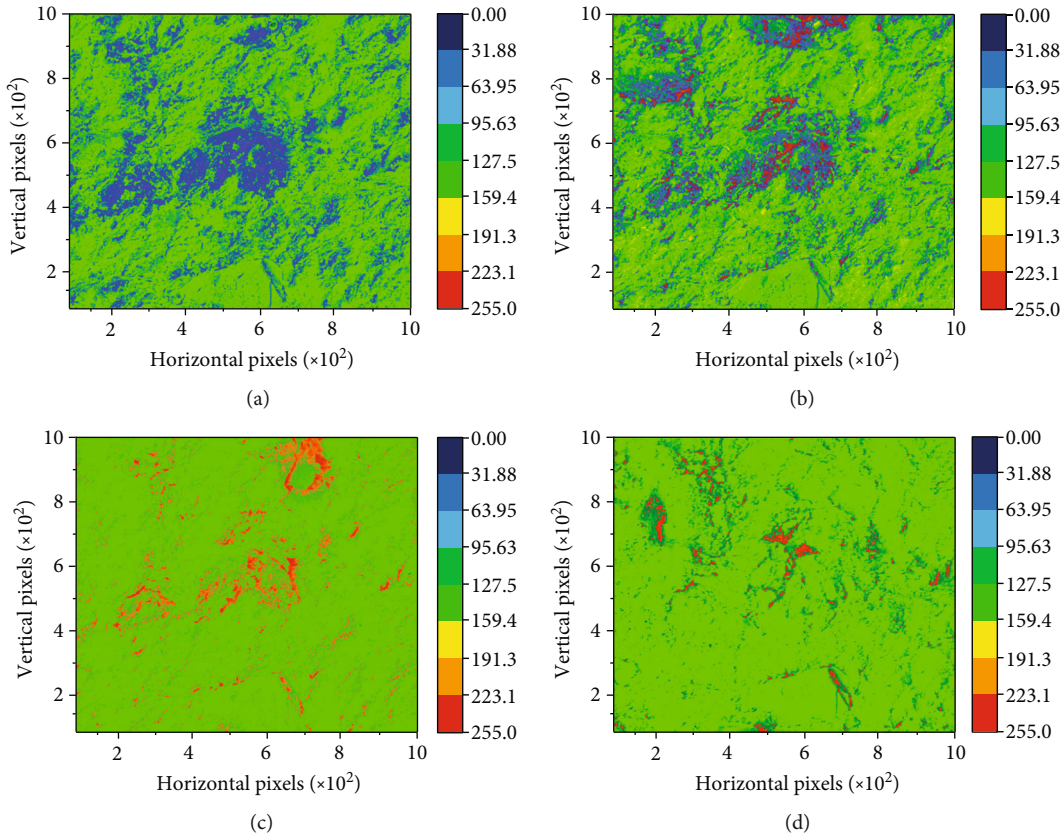

Figure 10: Color/gray distribution of oil shale before and after conduction-based heating. (a) Oil shale in initial state. (b) Oil shale at 300°C. (c) Oil shale at 400°C. (d) Oil shale at 500°C.

into four types according to diameter: micropores (<0.01 μm), pores (0.01~0.1 μm), mesopores (0.1 ~1 μm), and macropores (1 ~100 μm). The pore classification was obtained through analyses of the mercury injection test.

As the temperature increased during the conductive heating of oil shale sample No. I in Table 2 and Figure 13, the number of pores and the area of each pore increased. At 100°C ~300°C, the pores changed slowly. The volume of micropores decreased sharply at 300°C, and the distribution of the pores changed. The number of pores with a single pore circumference of 1 μm~2 μm increased, indicating that pores with diameters of 0.3 μm~1 μm were conducting. After heating, the average porosity increased from 4.95% to 5.20%, a 1.05-fold increase. The average perimeter of the pores increased from 2.342 μm to 2.874 μm, a 1.23-fold increase. The pore volume of small pores, mesopores, and large pores increase slowly, mainly micropores and small pores. This is mainly because organic matter begins to transform into hot pitch through physical and chemical changes, and the hot pitch produced blocks the micropores and small pores; at 400°C, the number of pores decreases, and the perimeter of single pores is similar to that at 300°C, but compared to 300°C, the pore size distribution is more uniform, mainly distributed in 1 μm~2 μm; the porosity increases slowly, and the average porosity increases from 4.950% to 11.173%, an increase of 2.26 times; the average perimeter of the hole decreased from 2.874 μm to 1.872 μm, a decrease of 0.799 times The volume of micropores decreased and that of small pores remained unchanged, but the volume of individual mesopores increased significantly. This was the stage in which hot asphalt was converted into oil and gas and blocked the micropores. At 500°C, the number of internal micropores and pores increased sharply. The volume of a single pore increased significantly from 1 μm~2 μm to 1 μm~ 3 μm, indicating that the number of small pores had gradually increased. Some small pores connected with each other to form mesopores. The average porosity was 19.137%, an increase of 3.87 times; the average perimeter of the holes was 4.231 μm, an increase of 1.85 times. The pores were spherical or ellipsoid, and some were irregular. The oil and gas in the oil shale sample along the seepage channel precipitated, and the pores expanded significantly. A large number of micropores connected to form new, larger pores, and the phenomenon of pore plugging gradually disappeared. This led to a rapid decrease in the number of micropores. The proportion of mesopores increased significantly, cracks began to appear, the organic matter in the oil shale was completely pyrolyzed, and changes in the pores of the oil shale became more prominent.

Due to the selective and uniform microwave heating, specimen No. III was completely different from specimen No. I (conductive heating) in Table 3 and Figure 14. At 100°C ~300°C and 350°C, the distribution of the pores changed. The number of pores with a circumference of 1 μm~2 μm increased, as did the porosity of a single pore, indicating that pores diameters of 0.3 μm~1 μm had begun

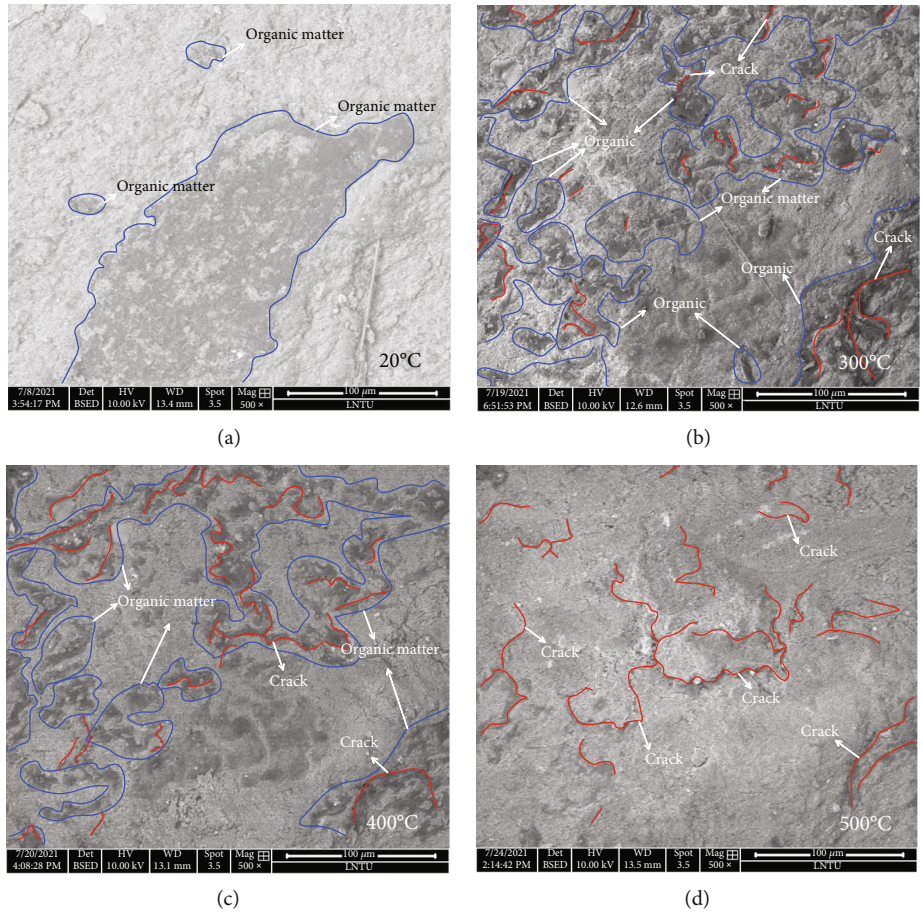

Figure 11: Scanning electron microscopy images of oil shale before and after microwave heating. (a) Oil shale in initial state. (b) Oil shale at 300°C. (c) Oil shale at 400°C. (d) Oil shale at 500°C.

to develop after microwave heating. The average porosity increased from 5.142% to 10.11%, an increase of 1.97 times, and the average perimeter of the pores increased from 1.278 μm to 2.879 μm, an increase of 2.253 times. The numbers of micropores and small pores grew slowly, as did the pore volume, and the organic matter was transformed into hot asphalt. Although the hot asphalt blocked the pores, the selective and uniform microwave heating caused the temperature of the area free of organic matter to rise more quickly. At 400°C, the number of pores increased sharply, the perimeter of a single pore increased from 1 μm~ 3 μm to 2 μm~ 4 μm, and the porosity of a single pore increased. The average porosity was 20.427%, an increase of 3.972 times. The average perimeter of the pores was 3.513 μm, an increase of 2.74 times. Owing to the intense microwave-induced pyrolysis reaction, the connectivity of the pores increased and cracks began to appear. Sample No. III began to appear flaky along the direction of bedding. The output in terms of organic matter was the largest, reaching 74% of the total output. At 500°C, the distribution of pore size increased, the perimeter of the pores increased from 2 μm~ 4 μm to 3 μm~ 6 μm, the porosity of a single pore continued to increase, and the average porosity was 24.137%, an increase of 4.69 times. The average perimeter of the pores was 5.741 μm, an increase of 4.49 times. The volume of mesopores and macropores gradually increased mainly due to the transition from the original micropores. Large pores were clear, and the pyrolysis reaction of oil shale was complete.

The analysis in Figure 15 shows that the porosity of the oil shale samples underwent significant changes using the two heating methods. The average porosity of the samples subjected to conductive increased from 4.950% to 19.137%. The average perimeter of the pores increased from 2.342 μm to 4.231 μm, an increase of 1.85 times. The average porosity of samples subjected to microwave heating increased from 5.142% to 24.137%, an increase of 3.69 times. The average circumference increased from 1.278 μm to 5.741 μm, an increase of 3.49 times. These results indicated that the pores and cracks of the oil shale samples subjected to microwave heating were more developed than those subjected to conductive heating, which improved pore connectivity.

4. Discussion

Microwave radiation heating is different from the conduction heating of the surface and the inside through an external heat source, but the volume heating of the heating object due to dielectric loss in the electromagnetic field

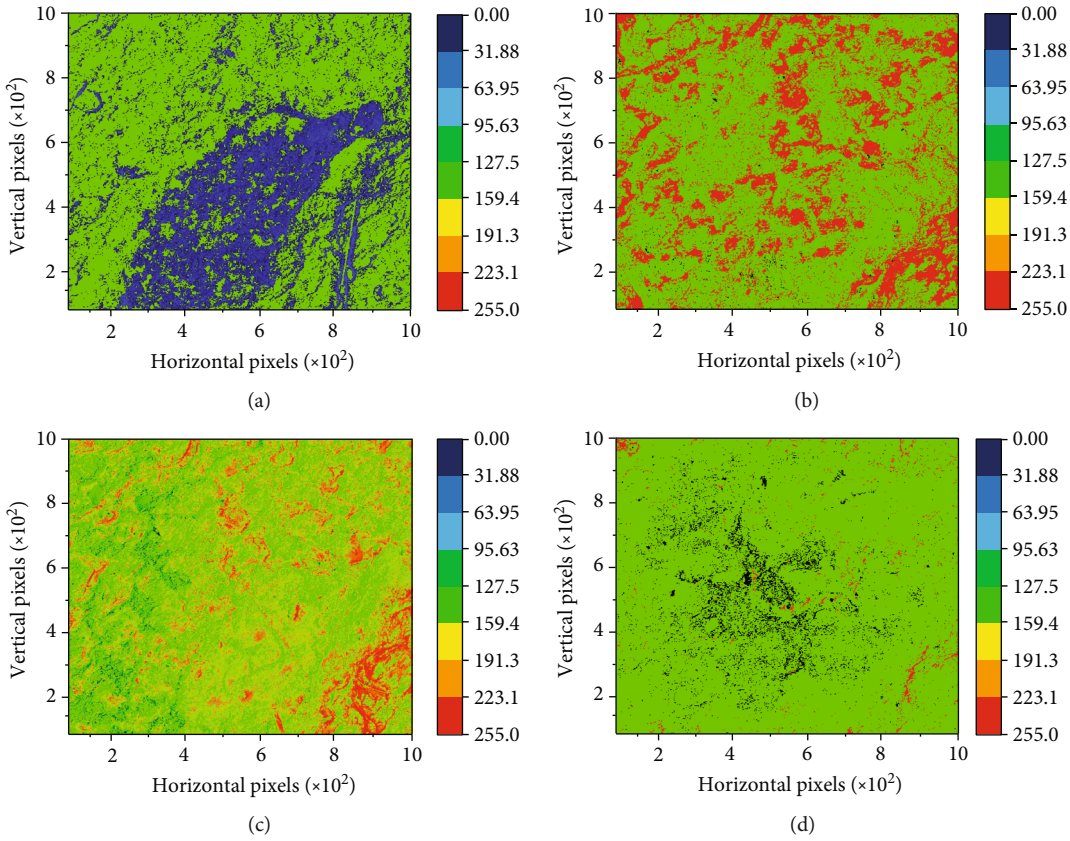

Figure 12: The color/gray distribution of oil shale before and after microwave heating. (a) Oil shale in initial state. (b) Oil shale at 300°C. (c) Oil shale at 400°C. (d) Oil shale at 500°C.

Table 2: Data on holes before and after conductive heating.

Sample type	Hole counting point	Average porosity (%)	Average hole perimeter (μm)
Initial state oil shale sample	826	6.620	1.574
After conduction-based heating at 300°C	517	11.271	2.139
After conduction-based heating at 400°C	488	14.705	1.759
After conduction-based heating at 500°C	1,057	20.966	3.486

[32]. When microwaves enter the medium in the form of a plane wave, a magnetic field is formed inside the medium, and polar molecules in it yield dielectric loss under the action of the high-frequency electromagnetic field. This converts electromagnetic field energy into heat energy. The dielectric loss of the polar molecules in the microwave field occurs mainly due to dipole turning polarization, and the time for the polarization establishment and elimination is between 10-6 s and 10-12 s. Therefore, polar molecules in the electromagnetic field are a source of quick microwave heating, and nonpolar molecules around the heat source are heated by conduction. Microwaves cause the oil shale to heat more evenly. The area of heat exchange was larger, solid organic matter in the oil shale was pyrolyzed more fully, and pores in the oil shale were quickly connected and expand.

The amount of dielectric loss is related to the dielectric constant of the medium. The permittivity of a lossy medium is as follows [33]:

$$\varepsilon = \varepsilon_0 \varepsilon_r = \varepsilon_0 \left(\varepsilon' - j\varepsilon''\right), \tag{1}$$

where ε_0 is the dielectric constant in vacuum, $\varepsilon_0 = 8.8542 \times 10^{12}$ (unit: F/m); ε_r is the relative dielectric constant of the medium; ε' is the real part of the dielectric constant, that is, the dielectric constant of the medium in the usual sense; and j is an imaginary unit. It is the imaginary part of the dielectric constant, that is, ε'', the loss factor. The larger the loss factor is, the stronger is the ability of the medium to absorb electromagnetic waves, and the easier it is to convert electrical energy into heat.

The energy of microwaves propagating in lossy media is absorbed and converted into heat. According to Abe's law in

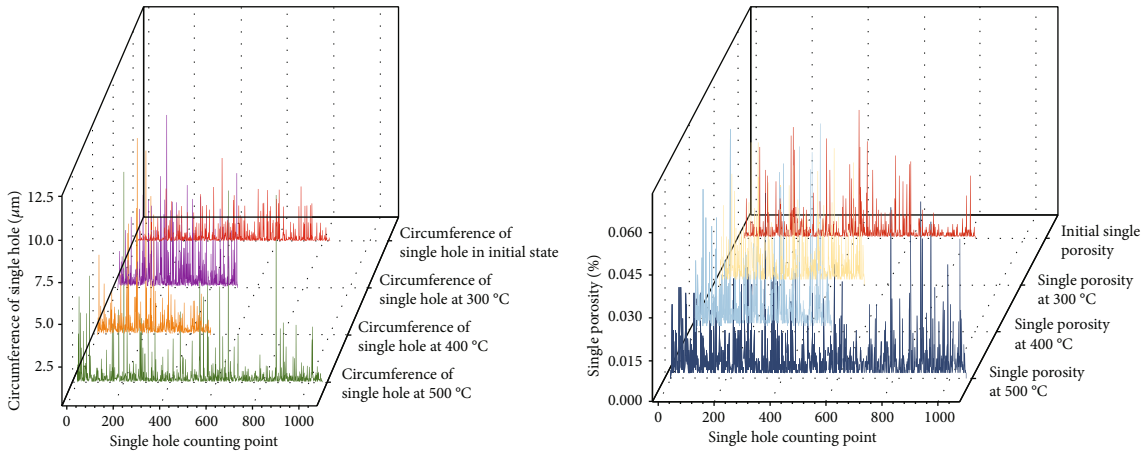

Figure 13: Changes in pores and cracks of oil shale under conductive heating. (a) Curve of changes in the perimeter of a single pore of oil shale. (b) Curve of changes in a single pore of oil shale.

Table 3: Data on holes before and after microwave heating.

Sample type	Hole counting point	Average porosity (%)	Average hole perimeter (μm)
Initial state oil shale sample	802	4.954	1.874
After microwave pyrolysis at 300°C	965	8.109	2.327
After microwave pyrolysis at 400°C	922	15.858	3.411
After microwave pyrolysis at 500°C	1,010	25.342	5.238

Maxwell's equation [34]:

$$\nabla \times H = J_e = \sigma E + j\omega\varepsilon E, \tag{2}$$

where ∇ is the Hamiltonian; H is the strength of the magnetic field (unit: V/m); J_e is the total current density (unit: A/m^2); σ is conductivity (unit: S/m); and ω is the frequency of the electromagnetic wave.

By substituting (1) into (2), all possible energy losses in the medium can be obtained:

$$J_e = j\omega\varepsilon_0\left[\varepsilon' - j\left(\varepsilon'' + \frac{\sigma}{\omega\varepsilon_0}\right)\right]E. \tag{3}$$

The dielectric loss factor in the actual medium consists of two parts: the loss of polarization of the dipole and Ohmic loss of conductance, expressed as

$$\varepsilon''_{eff} = \varepsilon'' + \frac{\sigma}{\omega\varepsilon_0}. \tag{4}$$

The lost microwave energy in the medium is converted into heat, thereby heating the medium. The loss of power in terms of dissipated energy is [35, 36]

$$P_{av} = \frac{1}{2}\omega\varepsilon_0\varepsilon''_{\text{eff}}E^2V. \tag{5}$$

Changes in the temperature of the medium caused by the conversion of microwave energy is affected by the parameters of medium, for which there is an endothermic formula [37]:

$$Q_c = M_aC_p\Delta T = \frac{P_{av}}{t}, \tag{6}$$

where Q_c is energy lost in the microwave medium, M_a is the mass of the medium, C_p is its specific heat, ΔT is the changes in temperature, and t is the duration of heating.

By substituting (5) into (6), the relationship between changes in temperature and the electric field strength and the dielectric constant can be obtained:

$$\Delta T = \frac{P_{av}}{M_aC_pt} = \frac{\omega\varepsilon_0\varepsilon''_{eff}E^2}{2\rho V}t. \tag{7}$$

It is clear from (7) that the temperature of the medium of microwave heating depended on the frequency of the microwaves, dielectric constant of the medium, and time.

When oil shale was heated by microwaves, a series of more complicated physical and chemical changes occurred in its interior than in case of conductive heating that directly affected and changed the pore structure of oil shale. This was mainly manifested in the following: (1) the selective and uniform heating by microwaves caused areas that did not contain organic matter to rapidly heat up, the number of pores increased, and the microwaves penetrated the pores to quickly pyrolyze the organic matter. (2) Pores generated after microwave heating increased the surface area of

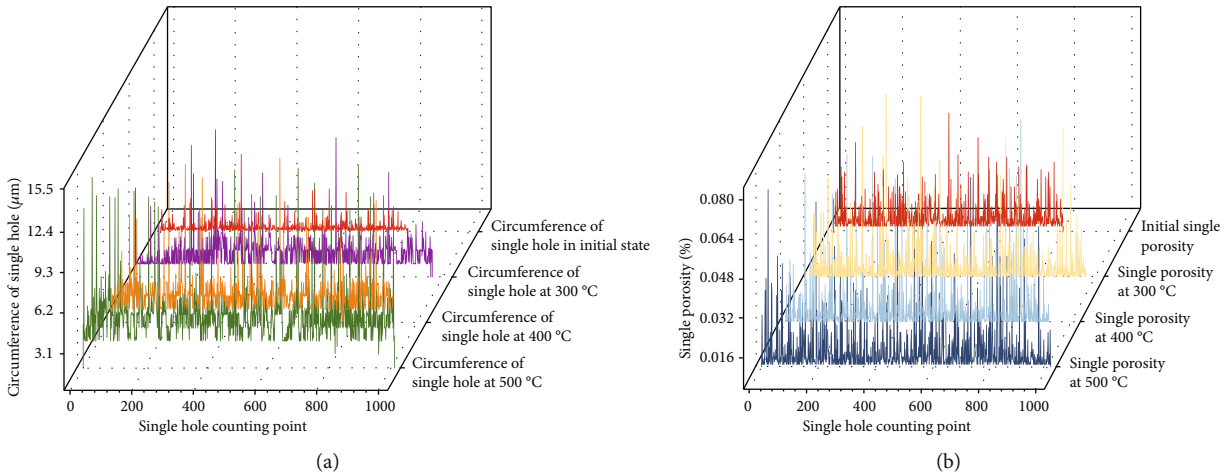

FIGURE 14: Changes in pores and cracks of oil shale under microwave heating. (a) Curve of changes in the perimeter of a single pore of the oil shale sample. (b) Curve of changes in a single pore of the oil shale sample.

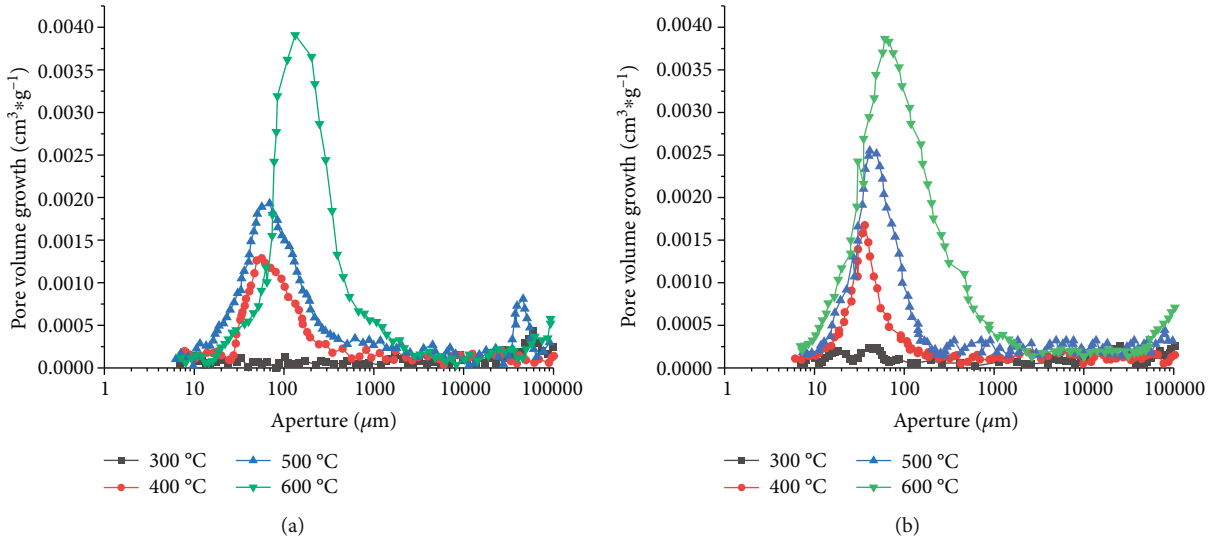

FIGURE 15: (a) Curve of the distribution of pore size of sample No. I. (b) Curve of the distribution of pore size of sample No. III.

microwave absorption. This caused the oil shale to react violently, increased its porosity, and led to the rapid production of shale oil and gas. (3) After microwave heating, the amount of semicoke produced decreased, as did the nitrogen and sulfur contents in the generated oil and gas was reduced. The quality of the oil and gas improved, which was convenient for subsequent refining. (4) As an efficient technology, microwave heating has many advantages in terms of speed, process control, quality of the pyrolysis product, and energy efficiency.

Figure 16 shows that at 100°C–300°C, the porosity of sample No. I increased from 6.62% to 11.27%. Its porosity at 300°C was 1.71 times than at 20°C. At 300°C to 500°C, the porosity of oil shale increased from 11.267% to 22.96%, and its porosity at 500°C was 3.4 times that at 20°C. The porosity of sample No. III increased from 4.95% to 10.11% at 100°C to 300°C, and at 300°C, it was 2.04 times that at 20°C. At 300°C to 500°C, the porosity of the sample increased sharply from 10.11% to 24.28%. Its porosity at 500°C was 4.9 times that at 20°C, significantly higher than that of the sample heated using conduction. After the sample was heated, a large number of new pore structures at various levels were generated due to the evaporation of adsorbed water, thermal decomposition of solid organic matter, and thermal cracking of the rock particles. This significantly increased the number of pores compared with the original sample. The porosity of specimen No. I rose slowly at 300°C ~ 400°C because organic matter was converted into asphalt due to heating. The asphalt blocked the pores to reduce porosity. However, the porosity of specimen No. III increased rapidly even when the hot asphalt blocked the pores. Above 400°C, the porosity of the sample increased, as did the connectivity between the pores. It was clear that organic matter was the main factor influencing the pyrolysis of oil shale. The degree of pyrolysis of organic matter was the most intense at 300°C ~ 500°C. Porosity increased sharply from 5.57% to 25.74% after heating. However, beyond 500°C, once the pyrolysis of kerogen in the organic matter

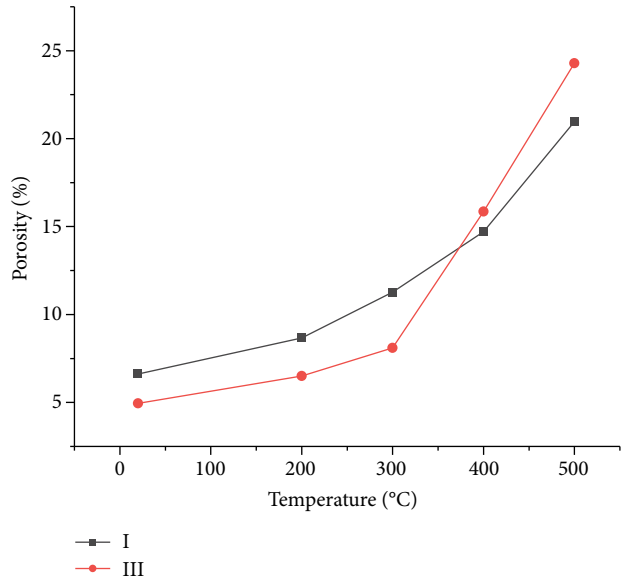

Figure 16: Curve of changes in the porosity of oil shale.

was complete, the rate of increase in porosity declined significantly.

In summary, microwave heating caused oil shale to heat evenly to generate a larger area of heat exchange. This caused solid organic matter in the oil shale to become more fully pyrolyzed and promoted the rapid expansion of pores in oil shale into large-scale pore connections. Microwave heating quickly pyrolyzed the hot bitumen originally blocked in the pores into oil and gas, which increased the fluidity of shale oil and gas. At the same time, it reduced the contents of nitrogen and sulfur in shale oil, which was convenient for subsequent refining.

5. Conclusions

This study conducted pyrolysis experiments on oil shale under different heating modes to analyze the evolution of its internal pore structure by using scanning electron microscopy, backscattering, and mercury intrusion tests. The following conclusions were obtained:

(1) Because the internal pores of oil shale were mostly closed "dead pores," its porosity did not increase significantly at a temperature of 100°C~200°C. The results of backscattering showed that the organic matter did not change at this temperature. This showed that organic matter was the main cause of pores in oil shale. The temperature was increased to open these closed pores to allow the products of pyrolysis to circulate, which enhanced the connectivity between pores

(2) When the pyrolysis temperature of oil shale was 300°C ~ 400°C, the increase in the number of micropores in the oil shale specimens decreased, mainly because the kerogen in the organic matter underwent a second-stage reaction to generate hot asphalt. The asphalt blocked the pores, resulting in a decrease in porosity. However, this phenomenon was not noted in the microwave pyrolysis of oil shale, mainly because the temperature rose relatively slowly to provide sufficient heat for the conversion of hot asphalt into oil and gas, and prevent blocking by hot asphalt. With the increase in temperature, the pyrolysis reaction of oil shale occurred, micropores in the oil shale specimens continued to increase in number, and the porosity of the samples continued to increase

(3) The microwave pyrolysis of oil shale required much less time than its conductive heating. As the microwave power was increased, the time required to reach the target temperature gradually decreased. The porosity of oil shale heated by conduction was 4.62 times the original porosity. The average porosity increased by 3.87 times from 4.950% to 19.137%, and the average perimeter of pores increased by 1.81 times from 2.342 μm to 4.231 μm. The porosity of oil shale heated by microwave radiation was 4.91 its original porosity. The average porosity increased by 4.69 times from 5.142% to 24.137%, and the average perimeter of pores increased by 4.49 times from 1.278 μm to 5.741 μm

Data Availability

The data used to support the findings of this study are available from the corresponding author upon request.

Conflicts of Interest

The authors declare that there are no conflicts of interest.

Authors' Contributions

All authors contributed to the conception and design of the study. Material preparation, data collection, and analysis were performed by Yao Cheng, Shan Lin, and Yulin Ma. The first draft of the manuscript was written by Yao Cheng, and all authors commented on previous versions of the manuscript. All authors read and approved the final manuscript.

Acknowledgments

This study was supported by the Liaoning Provincial Department of Education General Project (grant no. LJKZ0360) and by the Discipline Innovation Team Project of Liaoning Technical University (grant no. LNTU20TD-11).

References

[1] Q. Jialin, W. Jianqiu, and L. Shuyuan, "Utilization and development trend of world oil shale resources," *Journal of Jilin University (Earth Science Edition)*, vol. 6, pp. 877–887, 2006.

[2] Q. Jialin, W. Jianqiu, and L. Shuyuan, "Review of oil shale in the world," *Energy Of China*, vol. 8, pp. 16–19, 2006.

[3] L. Zhaojun, D. Qingshui, Y. Songqing et al., "Status quo of oil shale resources in China," *Journal of Jilin University (Earth Science Edition)*, vol. 6, pp. 869–876, 2006.

[4] Z. Kang, Z. Yangsheng, and Y. Dong, "Review of oil shale in-situ conversion technology," *Applied Energy*, vol. 269, article 115121, 2020.

[5] L. Wang, Y. Zhao, D. Yang, Z. Kang, and J. Zhao, "Effect of pyrolysis on oil shale using superheated steam: a case study on the Fushun oil shale, China," *Fuel*, vol. 253, pp. 1490–1498, 2019.

[6] Y. Zhao, Y. Wang, W. Wang, L. Tang, Q. Liu, and G. Cheng, "Modeling of rheological fracture behavior of rock cracks subjected to hydraulic pressure and far field stresses," *Theoretical and Applied Fracture Mechanics*, vol. 101, pp. 59–66, 2019.

[7] Y. Zhao, C. Zhang, Y. Wang, and H. Lin, "Shear-related roughness classification and strength model of natural rock joint based on fuzzy comprehensive evaluation," *International Journal of Rock Mechanics and Mining Sciences*, vol. 137, 2021.

[8] T. Saif, Q. Lin, B. Bijeljic, and M. J. Blunt, "Microstructural imaging and characterization of oil shale before and after pyrolysis," *Fuel*, vol. 197, pp. 562–574, 2017.

[9] P. Tiwari, M. Deo, C. L. Lin, and J. D. Miller, "Characterization of oil shale pore structure before and after pyrolysis by using X-ray micro CT," *Fuel*, vol. 107, no. 9, pp. 547–554, 2013.

[10] K. Zhiqin, L. Zhaoxing, Y. Dong, Y. Guochao, and Z. Yangsheng, "Study on solid-fluid-thermo-chemical coupling mathematical model for in-situ steam injection development of oil shale," *Journal of Xi'an Shiyou University (Natural Science Edition)*, vol. 4, p. 30-34+4, 2008.

[11] L. Zhijun, Y. Dong, H. Yaoqing, and S. Jixi, "Low-temperature nitrogen adsorption analysis of pore structure evolution of oil shale in situ pyrolysis," *Journal of Xi 'an University of Science and Technology*, vol. 38, no. 5, pp. 737–742, 2018.

[12] M. Qiaorong, K. Zhiqin, Z. Yangsheng, and D. Yang, "Thermal fracture and initiation mechanism test of oil shale," *Experiment on thermal Petroleum (edition of natural science)*, vol. 34, no. 4, pp. 89–92+98, 2010.

[13] F. T. Bai, Y. H. Sun, Y. M. Liu, and M. Guo, "Evaluation of the porous structure of Huadian oil shale during pyrolysis using multiple approaches," *Fuel*, vol. 187, pp. 1–8, 2017.

[14] K. E. Harfi, A. Mokhlisse, M. B. Chanaa, and A. Outzourhit, "Pyrolysis of the Moroccan (Tarfaya) oil shales under microwave irradiation," *Fuel*, vol. 79, no. 7, pp. 733–742, 2000.

[15] Z. Jianmei, S. Yonghui, L. Xinzhe, Z. Xicheng, and F. Jianping, "Effect of microwave power on oil shale pyrolysis," *Clean Coal Technology*, vol. 17, no. 5, pp. 66–69, 2011.

[16] B. Lee, Z. Dewen, F. Chaohe, and G. Zhixin, "Microwave redistillation is an effective method for shale oil development," *Natural Gas Industry*, vol. 32, no. 9, pp. 116–120+139-140, 2012.

[17] W. Qing, H. Xiankun, L. Hongpeng, S. Baizhong, and J. Chunxia, "Microwave dry distillation characteristics of Huadian oil shale," *Chemical Engineering Journal*, vol. 5, pp. 1288–1293, 2008.

[18] G. Wang, D. Yang, Y. Zhao, Z. Kang, J. Zhao, and X. Huang, "Experimental investigation on anisotropic permeability and its relationship with anisotropic thermal cracking of oil shale under high temperature and triaxial stress," *Applied Thermal Engineering*, vol. 146, pp. 718–725, 2019.

[19] L. Wang, D. Yang, and Z. Kang, "Evolution of permeability and mesostructure of oil shale exposed to high- temperature water vapor," *Fuel*, vol. 290, article 119786, 2021.

[20] Y. Yuan, J. Zhen-xue, C. Yu et al., *Characterization method of pore structure of shale*, CN105352873A, Beijing, 2016.

[21] M. E. Curtis, C. H. Sondergeld, R. J. Ambrose, and C. S. Rai, "Microstructural investigation of gas shales in two and three dimensions using nanometer-scale resolution imaging," *AAPG Bulletin*, vol. 96, no. 4, pp. 665–677, 2012.

[22] T. Saif, Q. Lin, A. R. Butcher, B. Bijeljic, and M. J. Blunt, "Multi-scale multi-dimensional microstructure imaging of oil shale pyrolysis using X-ray micro-tomography, automated ultra-high resolution SEM, MAPS Mineralogy and FIB-SEM," *Applied Energy*, vol. 202, pp. 628–647, 2017.

[23] Y. Zhao, Q. Liu, C. Zhang, J. Liao, H. Lin, and Y. Wang, "Coupled seepage-damage effect in fractured rock masses: model development and a case study," *International Journal of Rock Mechanics and Mining Sciences*, vol. 144, article 104822, 2021.

[24] M. V. Kok and A. G. Iscan, "Oil shale kinetics by differential methods," *Journal of Thermal Analysis and Calorimetry*, vol. 88, no. 3, pp. 657–661, 2007.

[25] Z. Kang, Y. Zhao, D. Yang, L. Tian, and X. Li, "A pilot investigation of pyrolysis from oil and gas extraction from oil shale by _in-situ_ superheated steam injection," *Journal of Petroleum Science and Engineering*, vol. 186, article 106785, 2020.

[26] C. S. Wen and T. P. Kobylinski, "Low-temperature oil shale conversion," *Fuel*, vol. 62, no. 11, pp. 1269–1273, 1983.

[27] L. Tiikma, A. Zaidentsal, and M. Tensorer, "Formation of thermobitumen from oil shale by low-temperature pyrolysis in an autoclave," *Oil Shale*, vol. 24, no. 4, pp. 535–546, 2007.

[28] S. H. Deng, Z. J. Wang, Y. Gao, Q. Gu, X. J. Cui, and H. Y. Wang, "Sub-critical water extraction of bitumen from Huadian oil shale lumps," *Journal of Analytical and Applied Pyrolysis*, vol. 98, pp. 151–158, 2012.

[29] X. M. Jiang, X. X. Han, and Z. G. Cui, "Mechanism and mathematical model of Huadian oil shale pyrolysis," *Journal of Thermal Analysis and Calorimetry*, vol. 86, no. 2, pp. 457–462, 2006.

[30] H. Pakdel, C. Roy, and W. Kalkreuth, "Oil production by vacuum pyrolysis of Canadian oil shales and fate of the biological markers," *Fuel*, vol. 78, no. 3, pp. 365–375, 1999.

[31] B. B. Hodot, *Outburst of Coal and Coalbed Gas*, S. Shizhao and W. Youan, Eds., China Industry Press, Beijing, 1966.

[32] H. Ming, P. Jinhui, W. Jiaqiang et al., "Theoretical study on the heating mechanism of the interaction between microwave and matter," *Journal of Kunming University of Science and Technology (Science and Technology Edition)*, vol. 6, pp. 15–17, 2005.

[33] W. Qing, H. Xiankun, K. Zhen, L. Hongpeng, and S. Baizhong, "Heating characteristics of oil shale and semi-coke in microwave field," *Journal of Microwaves*, vol. 25, no. 1, pp. 92–96, 2009.

[34] H. Guangze, C. Mingdong, G. Pingsheng, and L. Shaoxin, "Microwave absorption coefficient and power density of microwave-assisted extraction," *Journal of South China University of Technology (Natural Science Edition)*, vol. 4, pp. 52–57, 2007.

[35] M. E. C. Oliveira and A. S. Franca, "Microwave heating of foodstuffs," *Journal of Food Engineering*, vol. 53, no. 4, pp. 347–359, 2002.

[36] Y. Zhao, L. Zhang, J. Liao, W. Wang, Q. Liu, and L. Tang, "Experimental study of fracture toughness and subcritical crack growth of three rocks under different environments," *International Journal of Geomechanics*, vol. 20, no. 8, p. 04020128, 2020.

[37] A. K. Datta and R. C. Anantheswaren, *Handbook of Microwave Technology for Food Applications*, Marcel Dekker, Inc, New York, 2001.